EUROPEAN SPALLATION SOURCE
General ESS Meeting
October 16-19, 1995
Weinfelden, CH

Thermal Hydraulics of the ESS Liquid Metal Target

B. L. Smith
Thermal-Hydraulics Laboratory
Paul Scherrer Institute
Würenlingen and Villigen
Switzerland

Abstract

A two-dimensional, CFD[1] study has been initiated to examine the thermal hydraulic processes occurring in one design of the ESS liquid metal target. A progress report on this activity is presented in this article.

Introduction

One conceptual design for the ESS target [1] consists of a horizontal cylinder containing a liquid metal – mercury is considered in the present study – which circulates by forced convection and carries away the waste heat generated by the spallation reactions (Fig. 1). The protons enter the target via a beam window from the left, which must withstand the thermal, mechanical and radiation loads to which it is subjected. For a beam power of 5MW, it is estimated that about 3.3MW of waste heat is deposited in the target material and associated structures. The aim of the present study is to confirm, by detailed thermal-hydraulics calculations, that a convective flow of the liquid metal target material can effectively remove the waste heat and avoid any threat to the structural integrity of the target and its components due to overheating.

The target design adopted for the present study is shown in Fig. 2. The cylinder cross-section is elliptical and the beam window consists of an ellipsoidal dome of thickness 3mm, but tapering to 1.5mm at the centre. An internal flow guide directs cold liquid towards the window from below with a flow contraction near its exit to accelerate the flow over the window and promote efficient wall/fluid heat transfer. One idea to prevent the creation of a stagnant flow region on the outflow side is to make the flow guide perforated [2].

In this initial study, a two-dimensional model is employed which represents a vertical slice along the centre-line of the target. Conservative estimates are made concerning the beam heating power in order that the 2-D model represents a "worst-case" situation.

Numerical Model

Calculations are presented using two multi-purpose, transient fluid dynamics and heat transfer codes, ASTEC and CFDS-FLOW3D, both marketed by AEA Technology, based at Harwell [3,4]. The codes have been developed over many years and are used extensively in Europe and North America for the simulation of practical flow problems and as bases for the development of advanced physical models and computational techniques. A custom-built, interactive, grid-generator program (SOPHIA) is provided as part of the software package, together with a post-processor (JASPER) for the graphical display of results. The pre- and post-processors are fully compatible for the two codes, ensuring that the same mesh structure is maintained for the parallel ASTEC and FLOW3D simulations, and that a meaningful comparison of results can be made.

A 2-D finite-element-type mesh was created to model the target consisting of 6700 meshes, body-fitted to the target geometry, Fig. 3. The front and back faces are defined as symmetry planes and the model is made two elements thick to suppress motion in the third dimension. Note there are mesh concentrations towards the structure boundaries, particularly over the window surface, in order to resolve the expected temperature and

[1] Computational Fluid Dynamics

velocity gradients in the boundary layers adjacent to non-slip (heated) walls. For the last three calculations in the series the structure material of the cylindrical confinement (hull) is also represented. Five elements are used through the thickness to resolve the temperature gradient to the outside surfaces, which are treated as adiabatic boundaries. Note the thinning of the material towards the centre of the window.

The first calculations in the series examine the fluid flow characteristics of the system with the beam turned off; later simulations include heating effects. All calculations reported here are performed for a nominal inlet mass flow rate of 220 kg/s, equivalent to a mean inlet velocity of 1.6 m/s and an inlet Reynolds number close to 3.5×10^5. The high Reynolds number k-ϵ turbulence model with standard coefficients is used throughout. The flow outlet is assumed to be a constant pressure boundary.

Beam Heating

For the target design under consideration, the beam footprint is elliptical with a normalized, transverse power distribution

$$P(x,y) = \frac{2}{\pi x_o y_o}\left(1 - \frac{x^2}{x_o^2} - \frac{y^2}{y_o^2}\right),$$

with x_o(=3cm) and y_o(=10cm) the semi-minor and semi-major axes of the ellipse, respectively (Fig. 2). For the 2D simulation we use

$$P(x,y) = \frac{2}{\pi x_o y_o}\left(1 - \frac{x^2}{x_o^2}\right),$$

maintaining the parabolic distribution in the vertical x-direction, but uniform horizontally. In essence, we are analysing a thin vertical slice through the centre of the target and, since the beam heating is there a maximum, this represents a 'worst-case' scenario. Including the axial variation, the complete power density distribution in the mercury is given by:

$$P(x,y,z) = 6334\left(1 - \frac{x^2}{x_o^2}\right)\exp(-z/L_A)\left[1 - 0.7632\exp(-z/L_B)\right] \quad W/cm^3,$$

in which L_A=14.5cm is the attenuation length and L_B=6.55cm the build-up length. The power deposition in the window material is taken as

$$P(x,y) = 1000\left(1 - \frac{x^2}{x_o^2}\right) \quad W/cm^3.$$

A simple heat balance calculation

$$\dot{Q} = \dot{m} c_p \Delta\bar{T} \tag{1}$$

for the given inlet mass flow rate, $\dot{m}$=220 kg/s, and specific heat, c_p=138 J/kgK, would result in an average temperature increase $\Delta\bar{T}$=184°.

Results

A number of calculations have been performed in a step-by-step process of increasing complexity and flow guide perforation ratios. Results for the cases considered are summarised in Table 1, with more explanation below.

Case A

This is the base case of the series. A target length of 200 mm was chosen (to minimise computer run time) and an impervious flow guide was assumed. The computed flow field is given in Fig. 4 and shows that, as would be expected, a large recirculation region has been formed behind the flow guide, on the outlet side. In fact, the region extends to the outlet, where some inflow is seen, indicating that the length of the model is inadequate for this simulation. The decrease in pressure associated with the venturi contraction at the end of the flow guide is not recovered on the expansion side and a residual pressure drop Δp = 0.026 bar remains between the inlet and outlet channels. Thus, if the flow guide were perforated, the pressure drop

Case No.	Target Length (mm)	Flow Guide Porosity	Recirculation Zone Length (mm)	Mass Flow over Window (%)
A	200	0.0	430	100
B	550	0.0	430	100
C	550	0.15 (z <550)	–	2
D	550	0.06 (z <550)	–	5
E	550	0.06 (z <50)	440	41
F	550	0.06 (z <300)	–	12
G	Case F above with hull structure			
H	Case F above with hull structure and heat			
I	Case E above with hull structure and heat			

Table 1: Cases Considered

would enable bleeding of the inlet flow through the flow guide wall, as proposed to suppress the formation of the recirculation region.

Case B

This is the same as the Case A above except that the target length has been extended to 550 mm to capture the entire recirculation zone. Velocity vectors and negative axial velocity contours are given in Fig. 5 for this case and show that the recirculation extends to a distance 430 mm from the window. Otherwise, the flow is similar to Case A. Hereafter, all calculations refer to this extended model, whether or not the recirculation region exists.

Case C

For this calculation the flow guide is made porous along its entire length with a uniform perforation ratio γ=0.15. The pressure drop through the pores of the plate is assumed to be of the form

$$\Delta p = \frac{1}{2}\rho\zeta u^2,$$

in which u is the superficial velocity; that is, $u = \gamma u_d$, with u_d the actual velocity through the perforations. The value of the friction coefficient, ζ=94, is derived from tables of hydraulic resistances [5].

There is now no recirculation region (Fig. 6), demonstrating that the concept of a bleed flow through the flow guide wall has achieved the desired result and improved flow efficiency. One sees that most of the pressure loss in flow guide channel occurs before the contraction. In fact, the mass flow over the window is reduced to 2% of the inlet flow, and is surely insufficient to maintain adequate window cooling. Clearly, better optimisation of the design is necessary.

Case D

For this variant the perforation ratio is reduced to γ=0.06, again assumed uniform along the entire length of the flow guide, and the friction coefficient increased to ζ=590 [5]. The calculation reveals that, despite the increased flow resistance through the flow guide wall, the mass flow discharge to the window increases only marginally to 5% of the inlet flow. Otherwise, the flow field is qualitatively similar to Case C. Evidently, there is too much flow leakage at the upper end of the flow guide which does not contribute to the elimination

of the recirculation zone and is then unavailable for target cooling.

Case E

Here, only the curved end of the flow guide is perforated, with a perforation ratio γ=0.06, and the remainder is considered impervious. With this arrangement, though the flow discharge to the window region is now 41% of the total flow, the recirculation on the downstream side has reappeared and is much the same length (440mm) as before. Clearly, some intermediate configuration must be sought.

Case F

For this calculation the flow guide is perforated over about half its length (z <300mm) with γ=0.6, as before, and solid thereafter. With this combination, the recirculation zone has again disappeared but the discharge flow to the window is reduced to 12% of the total flow which may not be sufficient to maintain effective window cooling.

Interestingly, some of the flow which permeates the end of the flow guide is swept over the window rather than towards the outlet (Fig. 7). This fluid, whilst in transit, is subjected to beam heating and therefore brings extra heat to the window area and forms a stratified mixing layer with the cooler fluid coming from below, via the flow guide. The combined effects could be undesirable and, anyway, rather complex.

Case G

This is a repeat of Case F above, except that the structural elements of the hull are included for the first time. The case is included in the series solely as a consistency check on the mesh development and no further elaboration is necessary.

Case H

We now examine heat transfer effects by turning on the beam power. As noted earlier, the mean temperature increase across the target has been calculated as 184°, based on simple heat balance considerations. The temperature contours in Fig. 8a show local heating considerably in excess of this value. The temperatures are given in Kelvin in the Figure, with an inlet temperature 293.15K (20°C). The peak temperature increase in the target material is 1272° and, in fact, the mean temperature increase from inlet to outlet is 382°. The increase over the theoretical value occurs because the perforations in the flow guide allow some of the coolant to by-pass the heated region, thereby reducing the effective mass flow rate in Eqn. (1).

Temperatures along the axis of the target are given in Fig. 8b, together with those on the upper and lower surfaces of the cylinder. The sharp decrease of about 72° around z=0 is the temperature drop from the outside to the inside of the beam window (thickness 1.5 mm). This should not pose any thermal stress problems for the window material and shows that the constriction at the throat of the flow guide, and the accompanying flow acceleration, maintains adequate window cooling. However, due to the essentially stagnant flow conditions in the body of the target, the overall temperatures are very high and the upper cylinder wall is clearly overheating.

Case I

In this variation, which is a repeat of Case E above but including heating effects, we examine the consequences of increasing the mass flow to the window even though, in the isothermal case, this induced a recirculation zone on the downstream side of the flow guide. Shaded temperature contours for this case are shown in Fig. 9a. Qualitatively, the results are similar to Case H above with peak temperatures in the bulk flow region where the beam heating is greatest, and local overheating on the upper cylinder wall. The peak temperature increase in the target material is 947°, which is 325° lower than for Case H. The mean temperature increase from inlet to outlet, 377°, is little changed, however.

Temperatures along the axis of the target and the upper and lower surfaces are displayed in Fig. 9b. Temperature peaks are generally 200° lower than the Case H and the temperature drop across the window is 71°, little changed from before. In broad terms, it may be stated that, in the present model, the increased mass flow to the window region has more than compensated for the reappearance of the recirculation zone.

Conclusions

First steps have been undertaken in the construction of a computer model to examine the thermal hydraulic behaviour of one design of the ESS liquid metal target. The principle of using a perforated flow guide to discourage the formation of a recirculating flow on the downstream side of the window has been confirmed by means of fluid dynamic computations, for a number of perforation ratios.

Further calculations have been performed which have included beam heating effects. The flow constriction at the throat of the flow guide channel induces a fast streaming of the fluid across the target window from the lower to the upper side. It is shown that this arrangement leads to adequate window cooling, even if only 12% of the inlet mass flow is available for this purpose. However, the stagnation region on the downstream side of the flow guide remains, where the beam heating of the liquid metal itself is a maximum. This leads to extreme temperatures near the axis of the target and overheating of the upper surface. Perforations in the guide tube sufficient to eliminate the recirculation zone allow too much of the flow to by-pass the heated region of the target and the net effect is to exacerbate the overheating problem.

Admittedly, the calculations are two-dimensional and conservative. In particular, natural circulation currents in the transverse plane will go some way to alleviating the high temperatures on the axis of the target. Three-dimensional calculations would need to be performed to quantify this effect, and perhaps parameter studies would then need to be undertaken to determine an optimum design. However, there remains a fundamental defect in the present design in that maximum beam heating occurs in the region of minimum flow, and this will always lead to local overheating. The present study indicates that it would be prudent to pursue alternative liquid metal target designs and try to combine the cross-flow window cooling arrangement with a forced convection flow down the centre of the target to deal with the bulk-heating effect. This idea will be pursued in future CFD studies.

References

1. Gardner, I. S. K., Lengeler, H. & Rees, G. H. *Outline Design of the European Spallation Neutron Source*, ESS 95-30-M, Sept. 1995.

2. Bauer, G. PSI Internal Memorandum, 31 July 1995.

3. ASTEC Release 4.2 User Manual, AEA Technology, Harwell, UK (Aug. 1992).

4. CFDS-FLOW3D Release 3.3 User Manual, AEA Technology, Harwell, UK (June 1994).

5. Idel'Chik, J. E. *Handbook of Hydraulic Resistance: Coefficients of Local Resistance and Friction*, AEC-tr-6630 (1966).

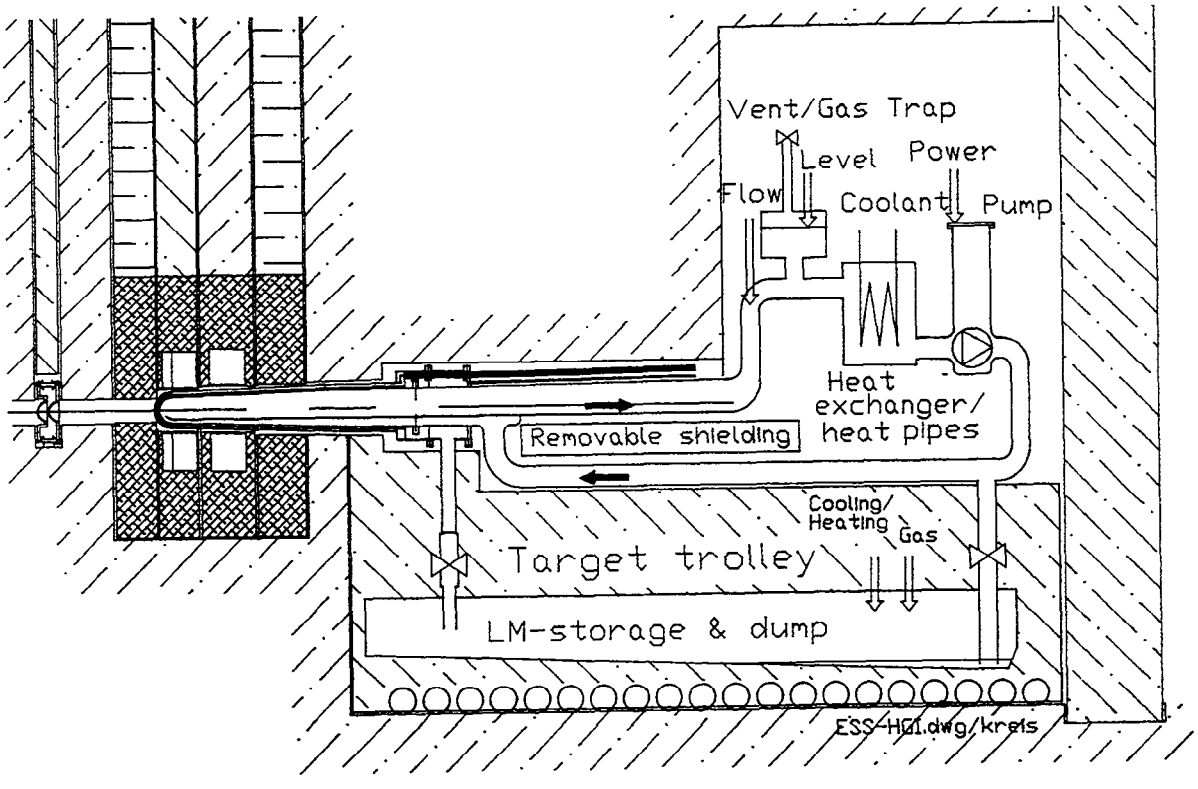

Figure 1: Schematic of ESS Liquid Metal Target Components

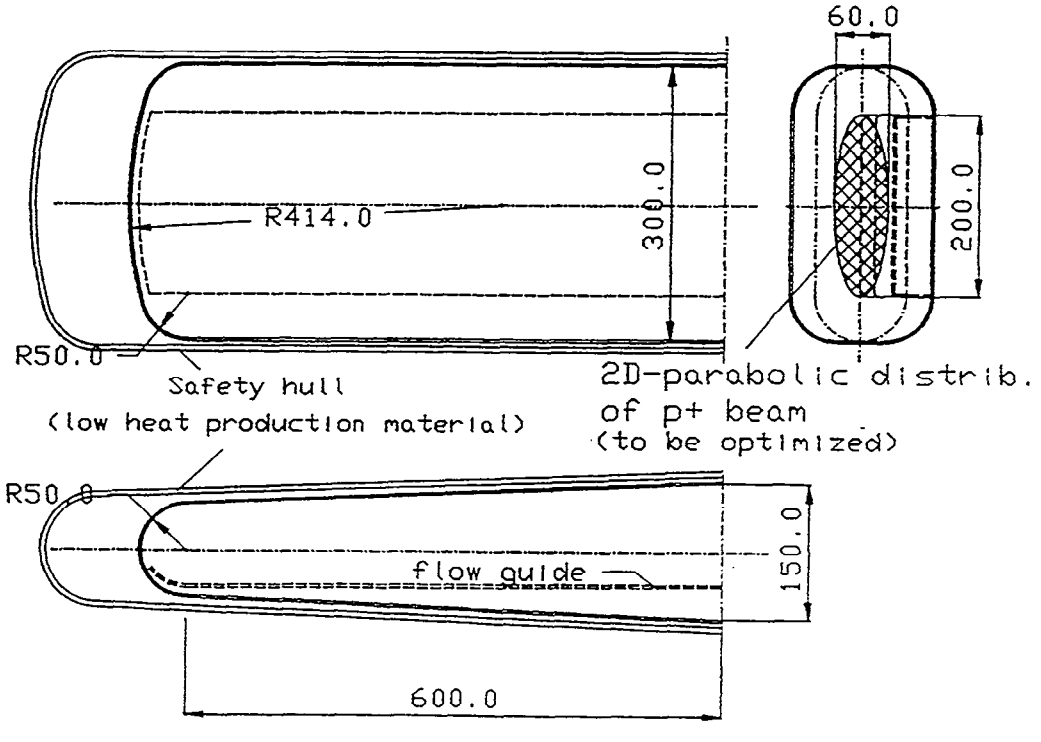

Figure 2: Proposed Target Geometry

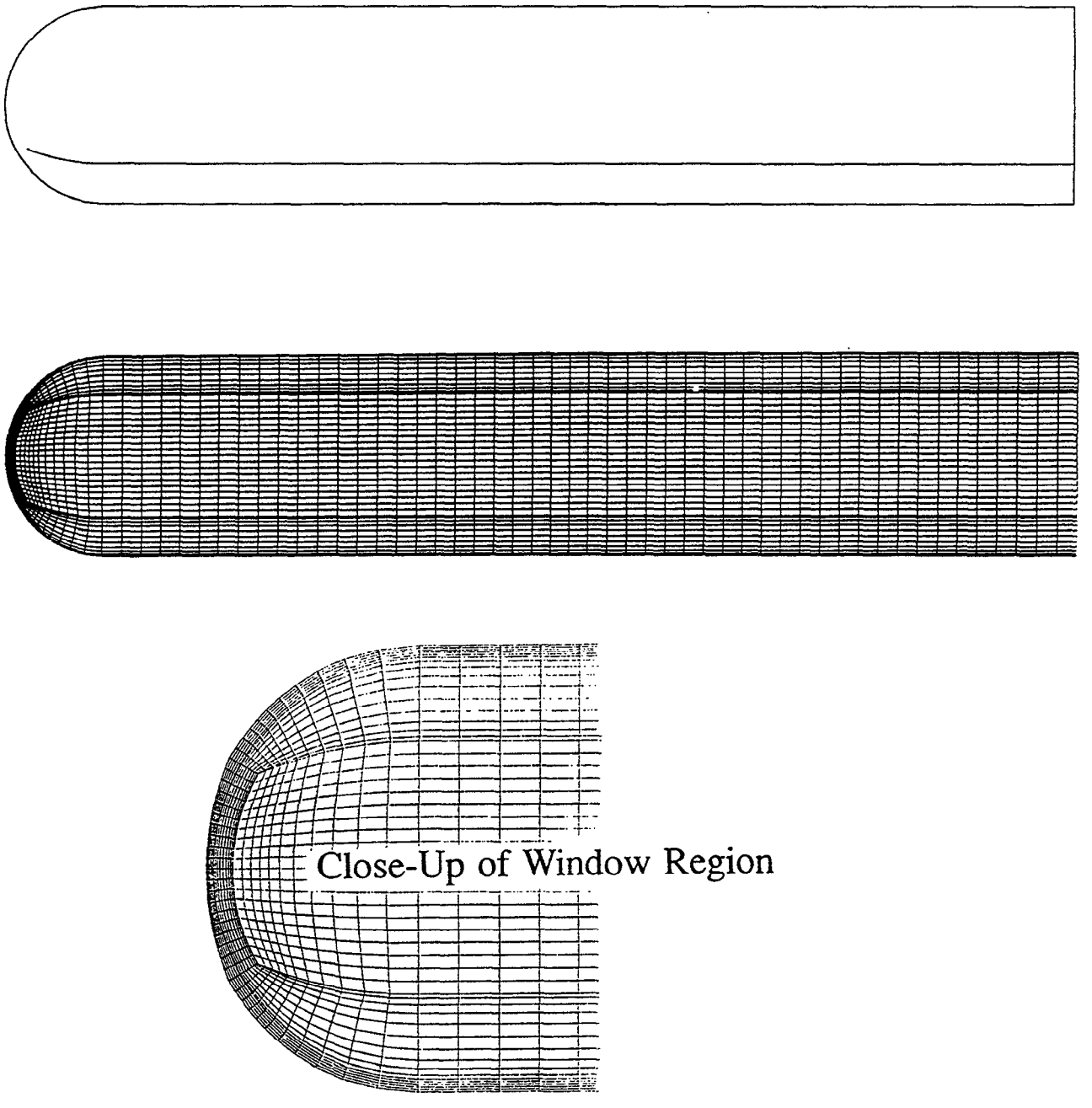

Figure 3: Mesh Geometry

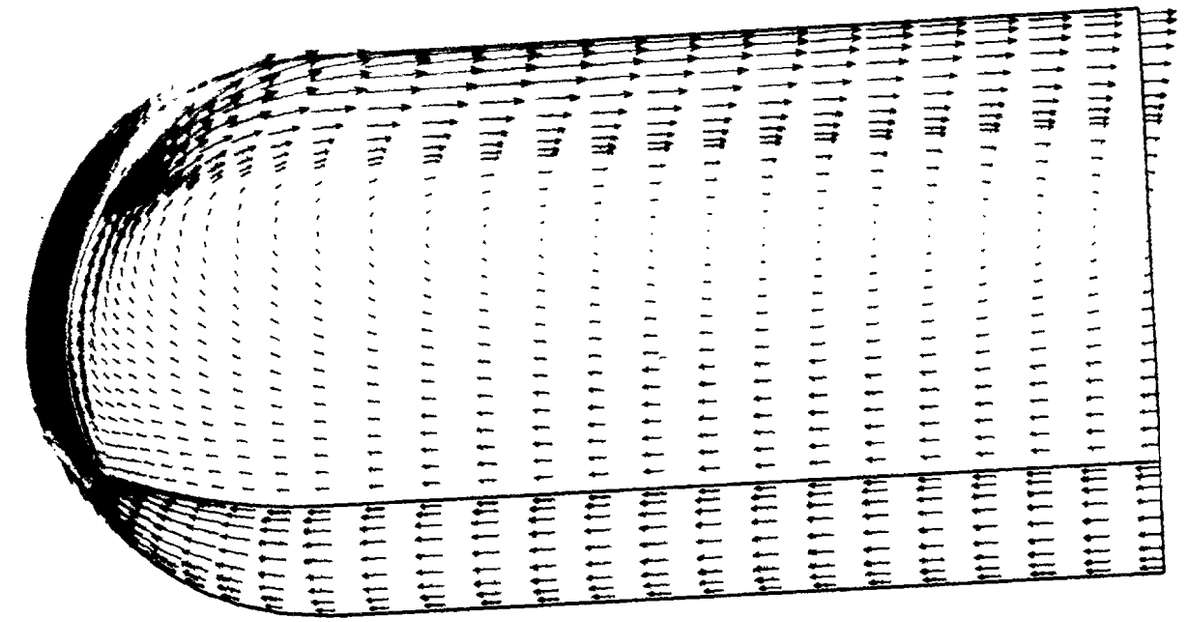

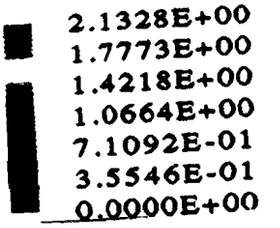

(a) Velocity Vectors

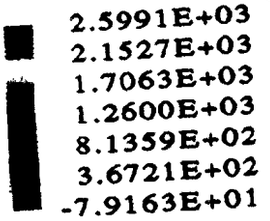

(b) Pressure Contours

Figure 4: Case A Calculation

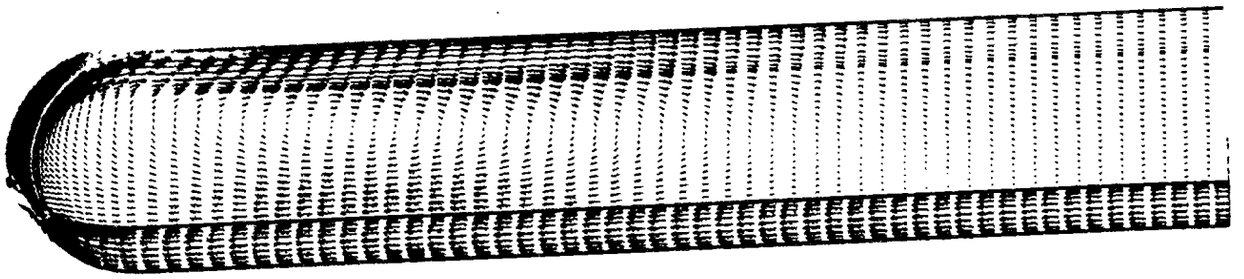

(a) Velocity Vectors

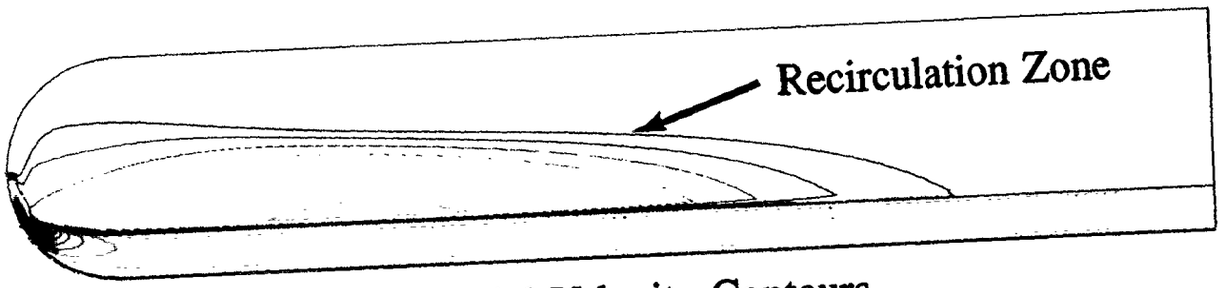

(b) Axial Velocity Contours

Figure 5: Case B Calculation

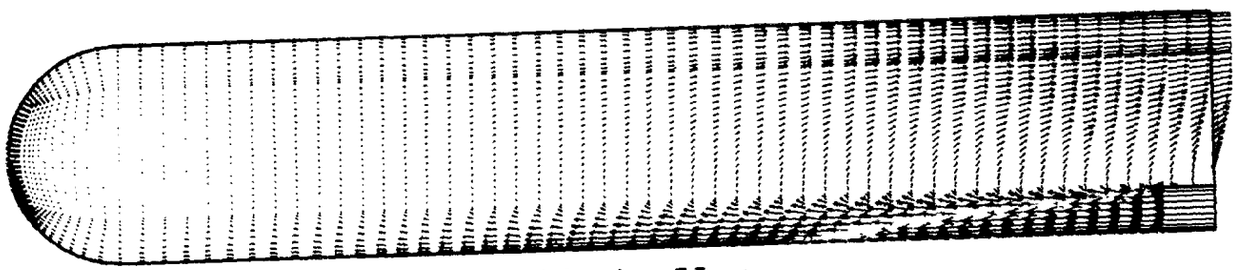

(a) Velocity Vectors

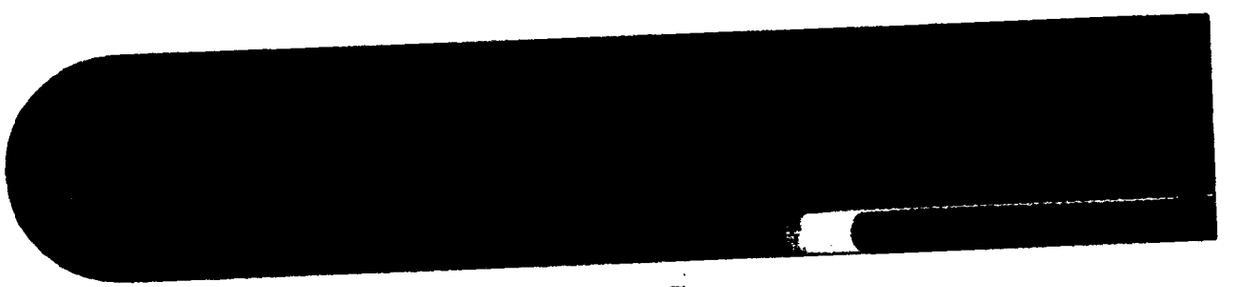

(b) Pressure Contours

Figure 6: Case C Calculation

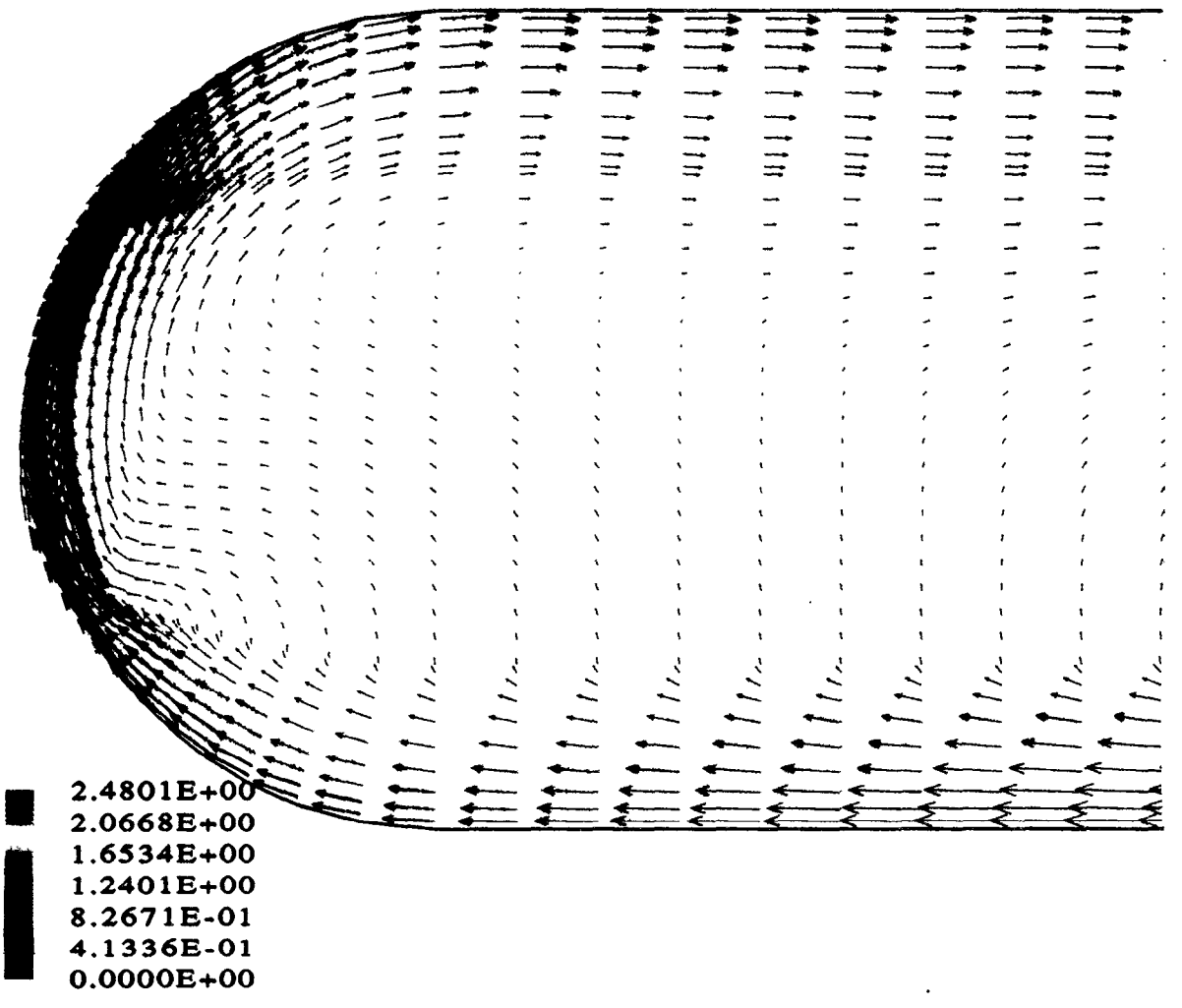

Figure 7: Case F Calculation
Details of the Flow in the Window Region

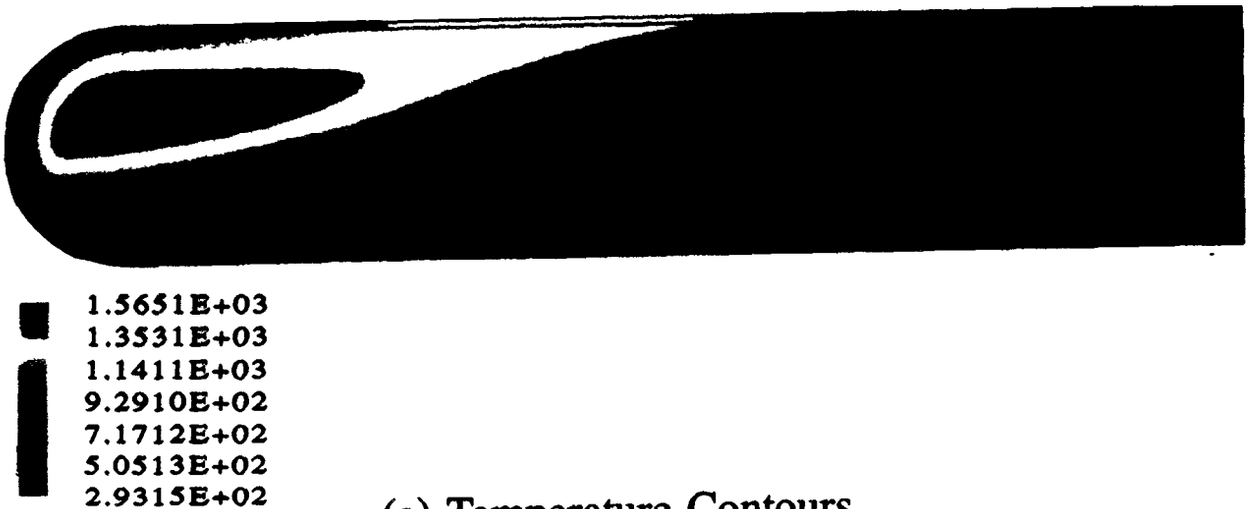

(a) Temperature Contours

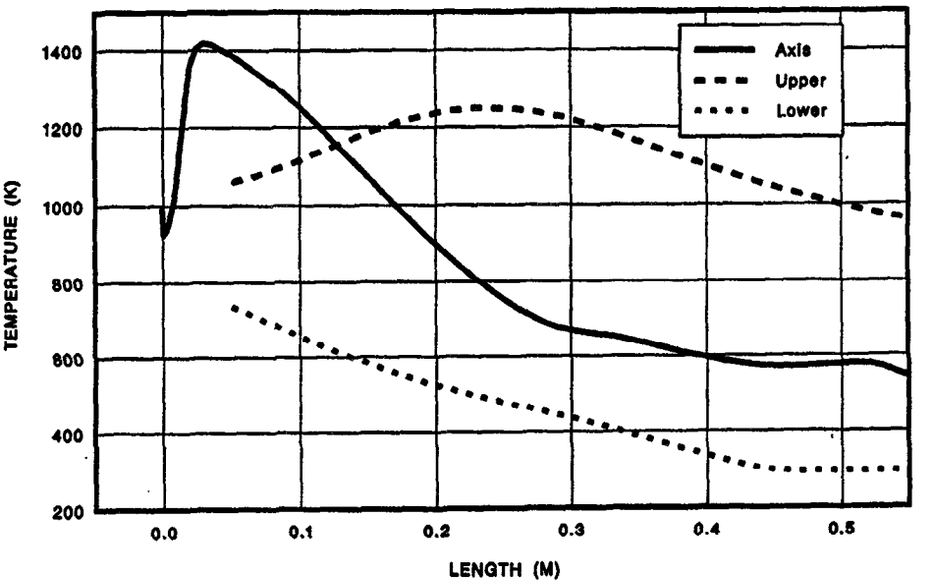

(b) Axial Temperature Distributions

Figure 8: Case H Calculation

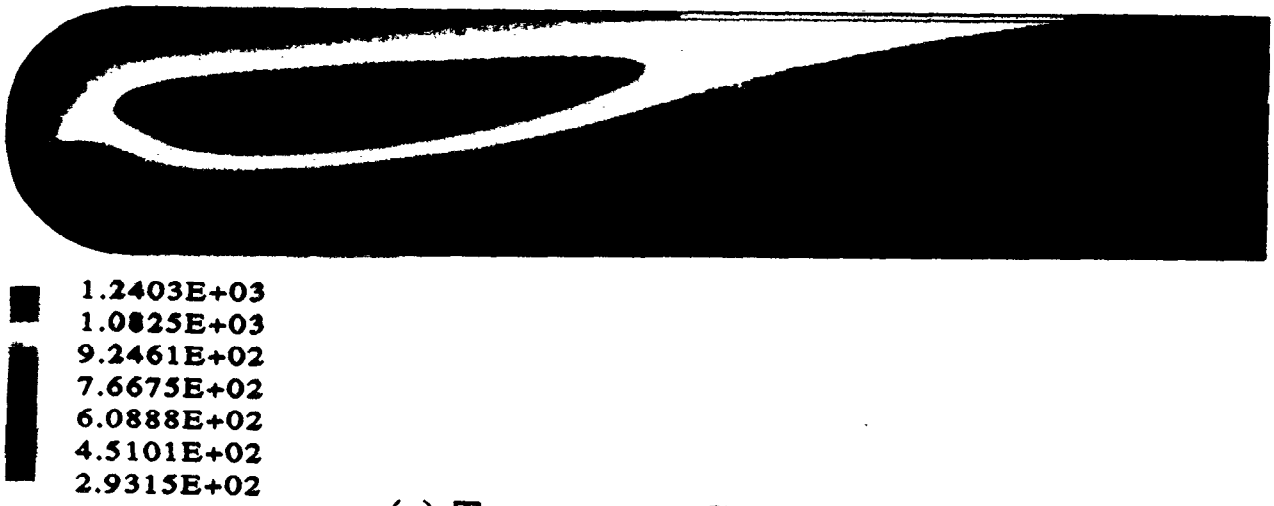

(a) Temperature Contours

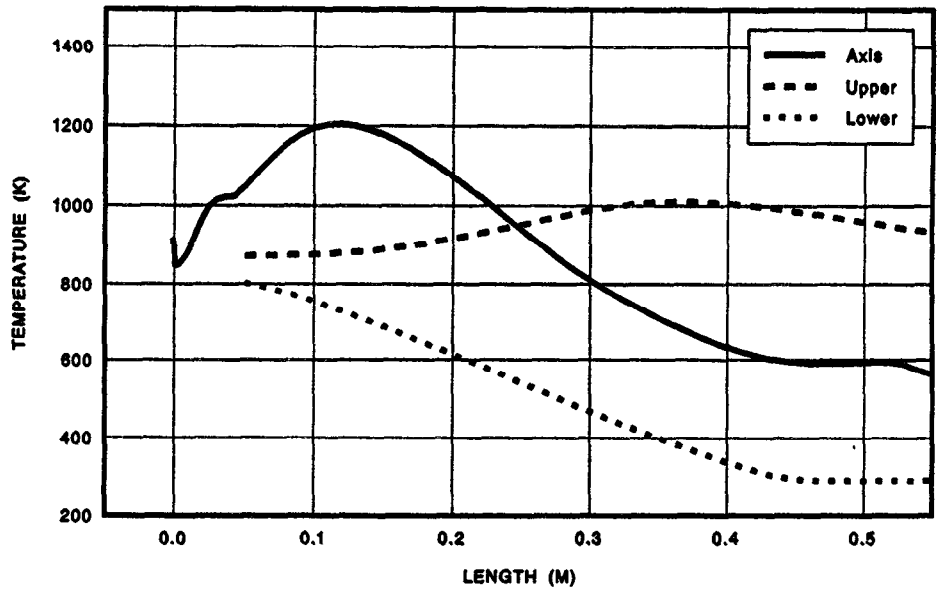

(b) Axial Temperature Distributions

Figure 9: Case I Calculation